Theoretical Studies of Elementary Hydrocarbon Species and Their Reactions

Final Technical Report DOE-UGA-15512

Wesley D. Allen and Henry F. Schaefer
Department of Chemistry and Center for Computational Quantum Chemistry,
University of Georgia

Performing Organization: University of Georgia Research Foundation

Date of Report: April 2018

Reporting Period: 5/15/16 – 11/15/17

DOE Grant Award Number: DE- SC0015512

Funding Office: DOE Office of Science, Basic Energy Sciences

Distribution Category: Unclassified and Unlimited

Final Technical Report DOE-UGA-15512

Date of Report: April 2018

Reporting Period: 5/15/16 – 11/15/17

DOE Grant Award Number: DE- SC0015512

Funding Office: DOE Office of Science, Basic Energy Sciences

Distribution Category: Unclassified and Unlimited

Theoretical Studies of Elementary Hydrocarbon Species and Their Reactions

Final Technical Report DOE-UGA-15512

Wesley D. Allen and Henry F. Schaefer
Department of Chemistry and Center for Computational Quantum Chemistry,
University of Georgia

April 2018

Unclassified research with unlimited distribution performed at the University of Georgia and funded by the U.S. Department of Energy, Office of Science, Basic Energy Sciences under grant award number DE- SC0015512 during the period May 15, 2016 through November 15, 2017.

ACKNOWLEDGEMENTS

The following scientists are acknowledged as co-authors appearing on the research publications supported by DOE grant number DE- SC0015512.

A. S. Abbott
J. Agarwal
G. Avila
U. Bozkaya
L. A. Burns
T. Carrington
E. Castro
R. E. Continetti
T. D. Crawford
A. E. DePrince
G. E. Douberly
M. Estep
F. A. Evangelista
P. F. Franke
A. Gao
J. F. Gonthier
E. G. Hohenstein
D. S. Hollman
P. R. Hoobler
A. M. James
R. A. King
A. Kumar
A. M. Launder
G. Li
D. Manogaran
S. Manogaran
S. Manzhos
H. R. McAlexander
K. B. Moore
C. P. Moradi
W. J. Morgan
J. W. Mullinax
K. V. Murphy
C. Ochsenfeld
S. K. Pandey
R. M. Parrish
K. Patkowski
B. Peng
B. P. Pritchard
H. Quanz
A. W. Ray
R. D. Remigio
R. M. Richard
H. I. Rivera-Arrieta
K. Sadeghian
M. Saitow
P. R. Schreiner
B. B. Shen
C. D. Sherrill
E. L. Sibert
A. C. Simmonett
D. G. A. Smith
A. Y. Sokolov
Z. Sun
D. P. Tabor
W. E. Turner
J. M. Turney
E. F. Valeev
P. Verma
N. A. Villegas-Escobar
X. Wang
A. T. Winkles
Y. Xie

Table of Contents

LIST OF FIGURES AND TABLES

SUMMARY

The research program supported by this DOE grant carried out both methodological development and computational applications of first-principles theoretical chemistry based on quantum mechanical wavefunctions, as directed toward understanding and harnessing the fundamental chemical physics of combustion. To build and refine the world's database of thermochemistry, spectroscopy, and chemical kinetics, predictive and definitive computational methods are needed that push the envelope of modern electronic structure theory. The application of such methods has been made to gain comprehensive knowledge of the paradigmatic reaction networks by which the *n*- and *i*-propyl, *t*-butyl, and *n*-butyl radicals are oxidized by O_2. Numerous ROO and QOOH intermediates in these R + O_2 reaction systems have been characterized along with the interconnecting isomerization transition states and the barriers leading to fragmentation. Other combustion-related intermediates have also been studied, including methylsulfinyl radical, cyclobutylidene, and radicals derived from acetaldehyde and vinyl alcohol.

Theoretical advances have been achieved and made available to the scientific community by implementation into PSI4, an open-source electronic structure computer package emphasizing automation, advanced libraries, and interoperability. We have pursued the development of universal explicitly correlated methods applicable to general electronic wavefunctions, as well as a framework that allows multideterminant reference functions to be expressed as a single determinant from quasiparticle operators. Finally, a rigorous analytical tool for correlated wavefunctions has been created to elucidate dispersion interactions, which play essential roles in many areas of chemistry, but whose effects are often masked and enigmatic. Our research decomposes and analyzes the coupled-cluster electron correlation energy in molecular systems as a function of interelectronic distance. Concepts are emerging that can be used to explain the influence of dispersion on the thermochemistry of large hydrocarbons, including fuels important to combustion technologies.

INTRODUCTION

The research program supported by this DOE grant was wide-ranging, including both methodological development and computational applications of first-principles theoretical chemistry. In the References section below, a total of 19 publications are listed whose research was supported by DOE grant number DE- SC0015512. Other projects initiated during the period of this report are continuing with the support of a successor grant DE-SC0018412. It is not practical to describe all of this research here, and we refer the reader to the listed publications for full details. In this report we have chosen to describe seven research highlights to demonstrate the scope and topics under investigation. Introductory material is given in each of these highlights as well as a synopsis of key findings.

RESEARCH HIGHLIGHTS

1. Integral Approximations and Screening for Studies on Large Molecules

The high computational cost of quantum electronic structure methods can be reduced by screening the ubiquitous two-electron repulsion integrals

$$g_{\mu\nu,\lambda\sigma} = \left(\mu\nu\middle|\lambda\sigma\right) = \int \chi_\mu(\mathbf{r}_1)\chi_\nu(\mathbf{r}_1)\frac{1}{r_{12}}\chi_\lambda(\mathbf{r}_2)\chi_\sigma(\mathbf{r}_2)d\tau_1 d\tau_2 \ , \tag{1.1}$$

where χ denotes atomic-orbital basis functions. The N^4 scaling with respect to basis set and molecular system size makes the full computation of the $g_{\mu\nu,\lambda\sigma}$ tensor prohibitive for very large molecules. In particular, the evaluation of this tensor is the limiting step for conventional Hartree-Fock (HF) and density functional theory (DFT) methods. The number of significant elements in this tensor that must be computed can be reduced (almost) to order N^2 using screening based on the Schwarz inequality

$$\left|\left(\mu\nu\middle|\lambda\sigma\right)\right| \le \sqrt{\left(\mu\nu\middle|\mu\nu\right)\left(\lambda\sigma\middle|\lambda\sigma\right)} \ . \tag{1.2}$$

However, for sufficiently large systems even this reduced cost is prohibitive, since the prefactor to the quadratic scaling is large. Furthermore, this prefactor grows rapidly with the quality of the one-electron basis set. Since realistic correlated computations usually require a basis set of at least triple-zeta quality, the usefulness of Schwarz-based screening can deteriorate quite rapidly in practical applications. Substantial effort has been invested in more aggressive screening techniques, but the inverse linear decay of the integration kernel in the general case severely limits the efficacy of such methods.

We have developed a local density fitting scheme in which atomic-orbital (AO) products are approximated using only auxiliary AOs located on one of the nuclei involved in that product. The possibility of spoiling the density fitting by variational collapse to an unphysical “attractive electron” state was alleviated by including atom-wise semidiagonal integrals exactly. Our approach leads to a significant decrease in the computational cost of density fitting for Hartree-Fock theory, while still producing results with errors 2-5 times smaller than standard, nonlocal

density fitting. Our method allows large Hartree-Fock and density functional theory computations with exact exchange to be carried out efficiently. We benchmarked our method on 200 large molecules, including up to 140 atoms. Our new fitting scheme leads to smooth and artifact-free potential energy surfaces and the possibility of relatively simple analytic gradients.

The electron repulsion integral (ERI) may equally well be expressed as

$$g_{AB} = \left(A \middle| B \right) = \int \Omega_A(\mathbf{r}_1) \frac{1}{r_{12}} \Omega_B(\mathbf{r}_2) d\tau_1 d\tau_2 \qquad (1.3)$$

where Ω_A and Ω_B are the (Mulliken notation) *bra* and *ket* charge distributions. For large molecules, the numerous (by far) contributors to the ERI tensor are the four-center cases, in which both Ω_A and Ω_B are product densities, composed of either atom-centered basis function in HF/DFT or molecular orbitals in correlated methods such as second-order perturbation theory. To reduce the computational cost of the four-center ERIs, Ω_A and Ω_B can be expanded in terms of an auxiliary basis set; the result density-fitting (DF) or resolution-of-identity (RI) approximation involves three- and two-center ERIs in which either or both of the *bra* and *ket* densities are single, atom-centered functions.

We have introduced a new estimator for three-center two-particle Coulomb integrals. Some performance data for this estimator are shown in Figure 1. Our estimator is exact for some classes of integrals and is much more efficient than the standard Schwartz counterpart due to proper account of distance decay. Although it is not a rigorous upper bound, the maximum degree of underestimation can be controlled by two adjustable parameters. We also have obtained numerical evidence of the excellent tightness of the estimator. The use of the estimator will lead to increased efficiency in reduced-scaling one- and many-body electronic structure theories. The above methodological advances would not have been possible (even with our relatively strong local computing situation) without major access to the DOE supported National Energy Research Scientific Computer Center (NERSC) at the Lawrence Berkeley Laboratory.

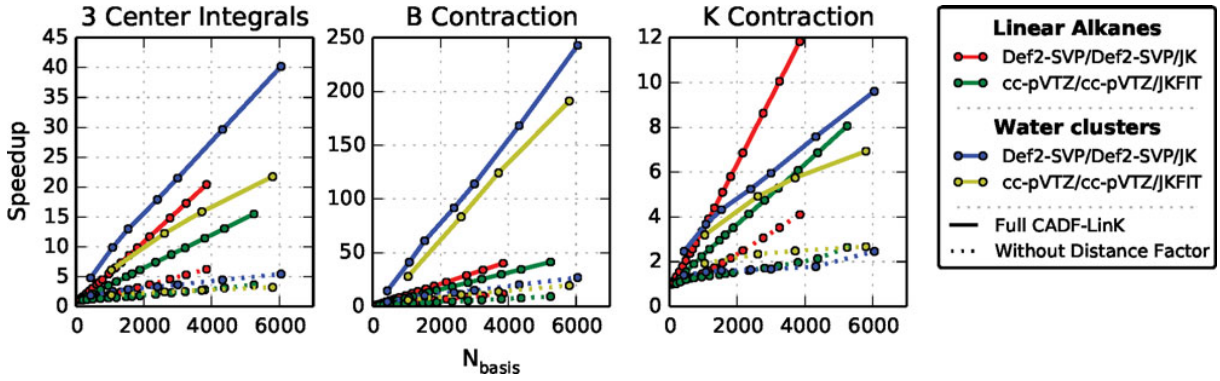

Figure 1. Performance of new estimator for three-center two-particle Coulomb integrals with and without the distance correcting factor. Speedup is relative to *a priori* screening based on the Schwarz inequality. Shown are speedups for the computation of the three-center integral, the B tensor contraction found in density-fitting methods, and the expensive exchange (K) contraction found in Hartree-Fock theory.

2. Quasiparticle Multireference Methods

The quasiparticle framework rests on existence of a unitary map $e^{\hat{\sigma}}$ connecting any multideterminantal reference wave function Ψ_0 to a single Slater determinant Φ, which allows the former to be expressed as a single determinant constructed from quasiparticle operators $\{\tilde{q}_i\} = \{\tilde{a}_p\} \bigcup \{\tilde{a}_q^\dagger\}$, where the tildes indicate transformation by $e^{\hat{\sigma}}$. Specifically,

$$\Psi_0 = e^{\hat{\sigma}} \Phi = \tilde{a}_1^\dagger \tilde{a}_2^\dagger \ldots \tilde{a}_n^\dagger \left| \widetilde{\text{vac}} \right\rangle \tag{2.1}$$

where

$$\hat{\sigma} = \hat{S} - \hat{S}^\dagger \tag{2.2}$$

and

$$\hat{S} = \sum_m \frac{1}{m!} \sum_{i_1 i_2 \ldots i_m} S(q_{i_1} q_{i_2} \ldots q_{i_m}) : \; q_{i_1} q_{i_2} \ldots q_{i_m} : \tag{2.3}$$

The multireference analogue of a dynamical correlation method is then obtained by representing the Hamiltonian in the basis of quasiparticle operators and using traditional single-reference algebra to derive working equations. Previous work by Sokolov and Chan used the Bogoliubov approximation, in which the target determinant is the vacuum state $\Phi = \left| \text{vac} \right\rangle$ and $\hat{S}$ is restricted to quadratic terms, to substantially extend the range of traditional MP2

methods in the presence of strong correlation at no additional cost.

After re-deriving the Bogoliubov quasiparticle Hamiltonian from first principles, we have derived and begun to implement a multireference variant of $CEPA_0$ (MR-$CEPA_0$) using this framework. The $CEPA_0$ method consistently outperforms CCSD near equilibrium, at reduced cost and improved parallelizability. However, like MP2, $CEPA_0$ rapidly breaks down away from equilibrium, limiting its range of applicability. Our Bogoliubov MR-$CEPA_0$ (BMR-$CEPA_0$) will provide a simple, effective extension of $CEPA_0$ in the presence of strong correlation. It requires only the one-particle density matrix of the reference wave function, which is readily obtainable for large systems using DMRG.

After applying the Bogoliubov approximation, spin-restricting with the condition $\left[\hat{S}_-, \tilde{a}^\dagger_{p\alpha}\right] \doteq \tilde{a}^\dagger_{p\beta}$ where $\hat{S}_-$ is the spin-lowering operator, and choosing the natural spin-orbitals of Ψ_0 as our reference orbitals, the Hamiltonian takes the following form in the quasiparticle basis:

$$\hat{H} = E_0 + v^q_p \tilde{a}^p_q + \tfrac{1}{4} v^{rs}_{pq} \tilde{a}^{pq}_{rs} + \hat{V} + \hat{V}^\dagger \tag{2.4}$$

in which

$$\hat{V} = \tfrac{1}{2} v_{pq} \tilde{a}^{pq} + \tfrac{1}{24} v_{pqrs} \tilde{a}^{pqrs} + \tfrac{1}{6} v^s_{pqr} \tilde{a}^{pqr}_s \,. \tag{2.5}$$

Our equations employ the Einstein summation convention, and we have defined

$$\tilde{a}^{p_1 p_2 \cdots p_m}_{q_1 q_2 \cdots q_k} \equiv \tilde{a}^\dagger_{p_1} \tilde{a}^\dagger_{p_2} \ldots \tilde{a}^\dagger_{p_m} \tilde{a}_{q_k} \ldots \tilde{a}_{q_2} \tilde{a}_{q_1} \,. \tag{2.6}$$

In contrast to Sokolov and Chan, we have defined the interaction tensors $v^{q_1 q_2 \cdots q_k}_{p_1 p_2 \cdots p_m}$ to be antisymmetric in their upper and lower indices and Hermitian in the sense $\left(v^{q_1 q_2 \cdots q_k}_{p_1 p_2 \cdots p_m}\right)^* = v^{p_1 p_2 \cdots p_m}_{q_1 q_2 \cdots q_k}$. By including the appropriate "equivalent line factors", $\frac{1}{m!k!}$, this enables the application of traditional diagrammatic methods.

The reference wave function is the transformed vacuum state $\left|\widetilde{\mathrm{vac}}\right\rangle = e^{\hat{\sigma}} \left|\mathrm{vac}\right\rangle \approx \Psi_0$, and the determinantal basis is $\left\{\left|\widetilde{\mathrm{vac}}\right\rangle\right\} \cup \left\{\left|\widetilde{pqrs}\right\rangle = \tilde{a}^\dagger_p \tilde{a}^\dagger_q \tilde{a}^\dagger_r \tilde{a}^\dagger_s \left|\widetilde{\mathrm{vac}}\right\rangle\right\}$. The BMR-CEPA0 energy and amplitude equations take the form:

$$E = \left\langle \widetilde{\mathrm{vac}} \right| \hat{H} \left(1 + \hat{C}_2\right) \left| \widetilde{\mathrm{vac}} \right\rangle \tag{2.7}$$

and

$$0 = \left\langle \widetilde{pqrs} \middle| \hat{H}\left(1+\hat{C}_2\right) \middle| \widetilde{\mathrm{vac}} \right\rangle \ , \tag{2.8}$$

where

$$\hat{C}_2 = \tfrac{1}{24} c_{pqrs} \tilde{a}^{pqrs} \ . \tag{2.9}$$

These equations an be evaluated algebraically or diagrammatically to give

$$E = E_0 + \tfrac{1}{24} v^{pqrs} c_{pqrs} \tag{2.10}$$

and

$$0 = P\left(p/qrs\right) v_p^t c_{tqrs} + \tfrac{1}{2} P\left(pq/rs\right) v_{pq}^{tu} c_{turs} \ , \tag{2.11}$$

in which *P* is the standard index permutation operator from traditional coupled cluster (TCC) theory. Separating v_p^q into diagonal and off-diagonal contributions, $v_p^q = \varepsilon_p \delta_p^q + v_p'^q$ where $\varepsilon_p \equiv v_p^p$ and $v_p'^q = \left(1-\delta_p^q\right) v_p^q$, we can set up an equation for Jacobi-like updating of the CEPA coefficients in an iterative procedure:

$$\left(\varepsilon_p + \varepsilon_q + \varepsilon_r + \varepsilon_s\right) c_{pqrs} = P\left(p/qrs\right) v_p'^t c_{tqrs} + \tfrac{1}{2} P\left(pq/rs\right) v_{pq}^{tu} c_{turs} \ . \tag{2.12}$$

The Hamiltonian in Eq. (2.4) and the amplitude conditions in Eq. (2.11) are actually much simpler than their analogues in TCC algebra. This is because the particle-hole isomorphism employed in TCC is built into the interaction tensors. Specifically, in the single-reference limit the Bogoliubov transformation becomes the particle-hole isomorphism between one's reference determinant Φ_0 and the vacuum $\left|\mathrm{vac}\right\rangle$.

3. Explicitly Correlated, Canonical Transcorrelated Methods

A barrier to achieving high accuracy in electron correlation computations is the slow convergence of the correlation energy with respect to the basis set size (basis set incompleteness error). Explicitly correlated R12/F12 methods address this problem by explicitly incorporating the interelectron distance (r_{12}) into the wave function ansatz. An alternative approach is the transcorrelated Hamiltonian of Boys and Handy that incorporates explicit correlation in an effective Hamiltonian. Recently, Yanai and Shiozaki proposed a canonical

transcorrelated (CT) Hamiltonian,

$$\hat{\bar{H}} = e^{\hat{A}^\dagger} \hat{H} e^{\hat{A}} \approx \hat{H} + \left[\hat{H}, \hat{A}\right]_{1,2} + \tfrac{1}{2}\left[\left[\hat{f}, \hat{A}\right]_{1,2}, \hat{A}\right]_{1,2}, \qquad (3.1)$$

that has the same complexity (only one- and two-body interactions) as the conventional electronic Hamiltonian, allowing the incorporation of this new method into existing electronic structure codes.

We have recently implemented the CT method using the code development tools in the PSI4 software package. Our initial implementation is written using the PSI4/Python interface, and we are currently writing an efficient C++ version of the CT method in PSI4, as well as adding new features such as novel F12 integrals. Our initial work in this area has focused on extensive benchmarking of the method, which is currently lacking in the literature. We have examined the dependence of the correlation energy with respect to Slater geminal exponents and compared CT results to those of popular F12 methods for small systems (Ne, HF, H_2O, NH_3). Continuing work will focus on using the CT Hamiltonian with higher-order coupled cluster methods such as CCSD(T), CCSDT, and CCSDT(Q). In addition to single reference coupled cluster studies, we are employing the CT approach into other methods that have been developed in our group such as density cumulant functional theory and the Mk-MRCC multireference coupled cluster theory.

4. The Multichannel *n*-Propyl + O_2 Reaction Surface

Reactions of alkyl radicals (R) with O_2 are paramount to low-temperature oxidation mechanisms involved in chemical phenomena such as autoignition and engine knock. Hydrocarbon (RH) oxidation processes are initiated through abstraction of an H atom (Eq. 4.1), preferentially from the weakest C–H bond. Initially, O_2 is apt to attack RH; however, as the hydroxyl radical pool builds, OH can become the predominant abstractor:

$$\mathrm{RH + Y \rightarrow R + YH} \qquad \mathrm{Y = O_2, OH, \ldots} \tag{4.1}$$

Barrierless addition of O_2 to R produces an alkylperoxy radical RO_2 (Eq. 4.2), which in turn drives the sequence of reactions given by Eqs. 4.3 – 4.10:

$$\mathrm{R + O_2 \rightleftharpoons RO_2} \tag{4.2}$$

$$\mathrm{RO_2 \rightarrow alkene + HO_2} \tag{4.3}$$

$$\mathrm{RO_2 \rightleftharpoons QOOH} \tag{4.4}$$

$$\mathrm{QOOH \rightarrow aldehyde + OH} \tag{4.5}$$

$$\mathrm{QOOH \rightarrow cyclic\ ether + OH} \tag{4.6}$$

$$\mathrm{QOOH \rightarrow alkene + HO_2} \tag{4.7}$$

$$\mathrm{QOOH + O_2 \rightleftharpoons OOQOOH} \tag{4.8}$$

$$\mathrm{OOQOOH \rightarrow OH + ketohydroperoxide} \tag{4.9}$$

$$\mathrm{ketohydroperoxide \rightarrow OH + alkoxy\ radical} \tag{4.10}$$

where QOOH is a carbon-centered hydroperoxyalkyl radical, and OOQOOH is an oxygen-centered hydroperoxyalkyl peroxy radical. Figure 2 gives a schematic potential energy surface (PES) of the *n*-propyl + O_2 reaction mechanism comprised of Eqs. 4.2 – 4.7.

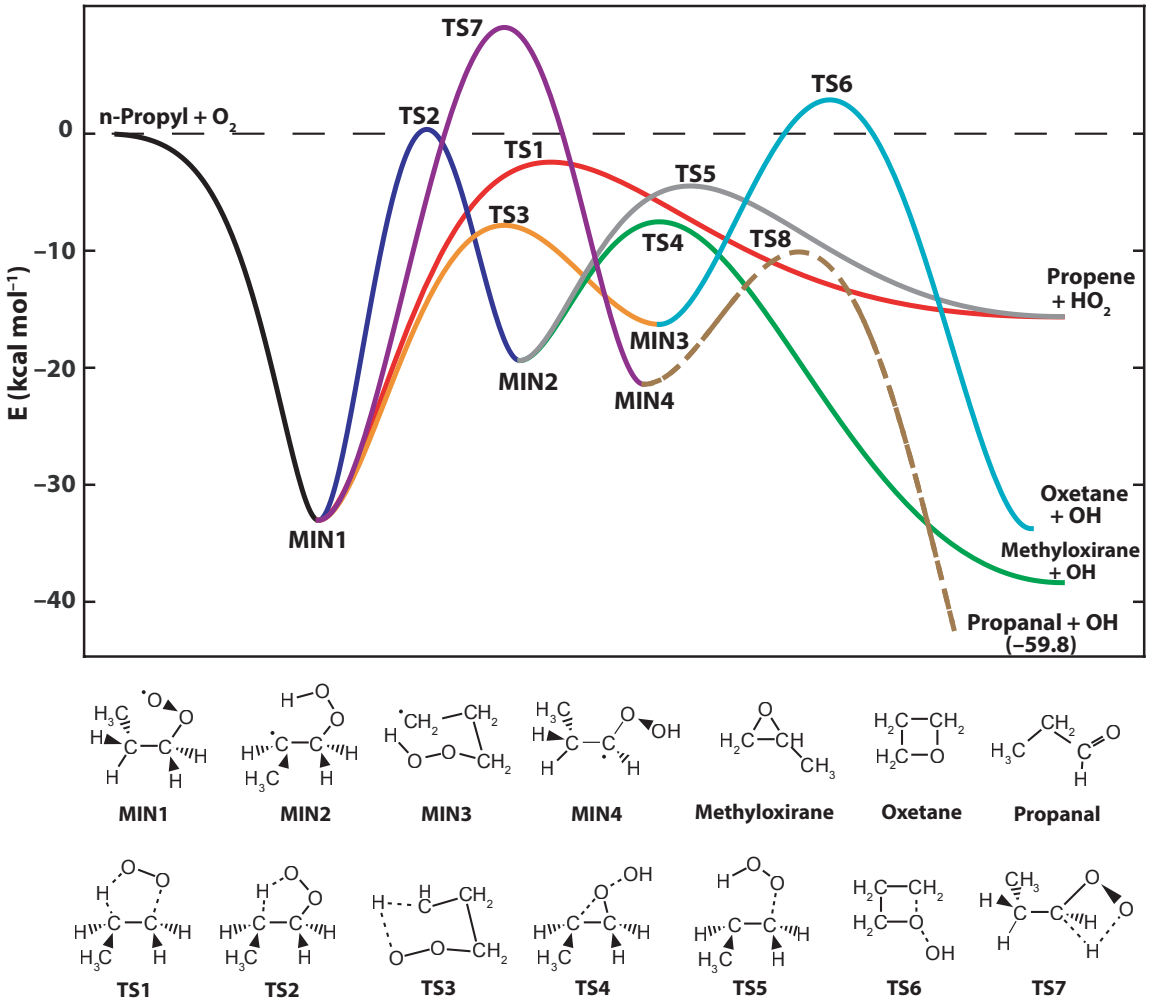

Figure 2. Schematic potential energy surface (PES) for *n*-propyl + O_2 reactions.

Multiple unimolecular transformations of stabilized RO_2 radicals are possible, including reverse fragmentation back to R + O_2, concerted elimination to produce an alkene + HO_2 (Eq. 4.3), and isomerization to form QOOH via hydrogen transfer (Eq. 4.4). The equilibrium of Eq. 4.2 lies well to the right in the region of 500-600 K, but at higher temperatures (T > 1000 K), the reaction shifts back to the separated reactants, removing the RO_2 chain carrier. Moreover, the concerted elimination step is effectively chain terminating at low temperatures, because HO_2 radicals are relatively unreactive. These two effects lead to a negative temperature coefficient (NTC) region, in which hydrocarbon reactivity decreases with increasing temperature. Finally, a complete kinetic model that reproduces all aspects of R + O_2 experiments must include not only

reactions (4.1) – (4.10) but also formally direct pathways from the reactants or each intermediate to every other intermediate or bimolecular product.

Because the *n*-propyl + O_2 reaction is an important model of chain branching reactions in larger combustion systems, we executed a comprehensive examination of this reaction system with definitive theoretical methods. Focal point analyses (FPA) extrapolating to the *ab initio* limit were performed based on explicit quantum chemical computations with electron correlation treatments through CCSDT(Q) and basis sets up to cc-pV5Z. All reaction species and transition states were fully optimized at the rigorous CCSD(T)/cc-pVTZ level of theory, revealing some substantial differences in comparison to the DFT geometries existing in the literature. A mixed Hessian methodology was implemented and benchmarked that essentially makes the computations of CCSD(T)/cc-pVTZ vibrational frequencies feasible and thus provides critical improvements to zero-point vibrational energies (ZPVE) for the *n*-propyl + O_2 system.

Two key stationary points, *n*-propylperoxy radical (**MIN1**) and its concerted elimination transition state (**TS1**), were located 32.7 kcal mol^{-1} and 2.4 kcal mol^{-1} below the reactants, respectively. The structure of **TS1** is shown in Figure 3, and the FPA analysis leading to the final prediction of the critical **TS1** barrier height is laid out in Table 1. Two competitive β-hydrogen transfer transition states (**TS2** and **TS2'**) were found separated by only 0.16 kcal mol^{-1}, a fact unrecognized in the current combustion literature. As shown in Table 2, our converged FPA energy places **TS2** only 0.37 kcal mol^{-1} above separated reactants. Incorporating **TS2'** in master equation (ME) kinetic models might reduce the large discrepancy of 2.5 kcal mol^{-1} between FPA and ME barrier heights for **TS2**. An anomalously large diagonal Born-Oppenheimer correction (Δ_{DBOC} = 1.71 kcal mol^{-1}) is exhibited by **TS2**, which is indicative of a nearby conical intersection of potential energy surfaces, as depicted in Figure 4. The first systematic conformational search of three QOOH intermediates of the *n*-propyl + O_2 system was completed, uncovering a total of 32 rotamers lying within 1.6 kcal mol^{-1} of their respective lowest-energy minima. Our definitive energetics for stationary points on the *n*-propyl + O_2 potential energy surface provide key benchmarks for future studies of hydrocarbon oxidation.

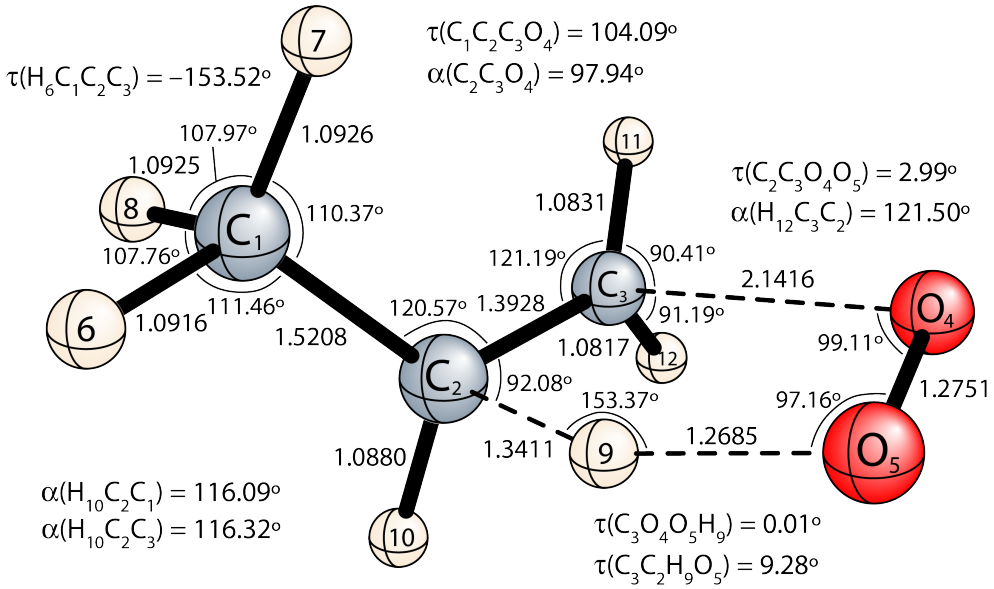

Figure 3. Optimum geometry of **TS1** of the *n*-propyl + O_2 at ROCCSD(T)/cc-pVTZ level of theory. Bond lengths in Å.

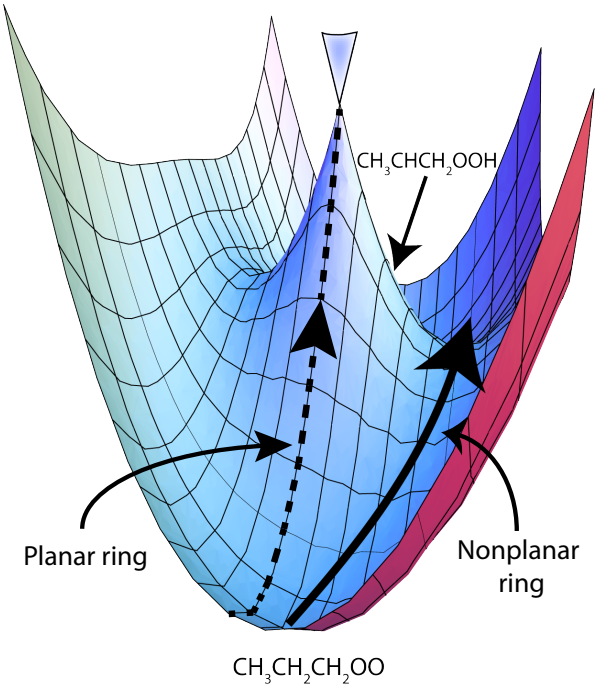

Figure 4. Qualitative depiction of the conical intersection of the *n*-propyl + O_2 potential energy surfaces near **TS2** and **TS2′**.

TABLE 1. Focal point analysis[a] (in kcal mol^{-1}) for the concerted elimination barrier (**TS1**) relative to *n*-propyl + O_2

	ΔE_e(ROHF)	+δ [ZAPT2]	+δ [ROCCSD]	+δ [ROCCSD(T)]	+δ [ROCCSDT]	+δ [UCCSDT(Q)]	NET
6-31G*	+34.72	–22.22	–2.99	–5.15	–0.22	–0.51	+3.64
cc-pVDZ	+32.57	–21.17	–3.04	–5.80	–0.07	[–0.51]	[+1.99]
cc-pVTZ	+33.19	–26.28	–1.18	–7.00	[–0.07]	[–0.51]	[–1.85]
cc-pVQZ	+33.34	–27.72	–0.75	–7.26	[–0.07]	[–0.51]	[–2.98]
cc-pV5Z	+33.37	[–28.24]	[–0.60]	[–7.35]	[–0.07]	[–0.51]	[–3.39]
CBS LIMIT	[+33.38]	[–28.78]	[–0.43]	[–7.45]	[–0.07]	[–0.51]	[–3.86]

FC-ROCCSD(T)/cc-pVTZ reference geometries

$\Delta E_{final} = \Delta E_e(\text{FPA}) + \Delta\text{ZPVE (harm)} + \Delta(\text{rel}) + \Delta(\text{core}) = -3.86 + 1.39 + 0.07 - 0.01 =$ **–2.41 kcal mol^{-1}**

[a] The symbol δ denotes the increment in the relative energy (ΔE) with respect to the preceding level of theory in the hierarchy HF→ZAPT2→ROCCSD→ROCCSD(T)→ROCCSDT→UCCSDT(Q). Square brackets signify results obtained from basis set extrapolations or additivity assumptions.

TABLE 2. Focal point analysis[a] (in kcal mol^{-1}) for the β-hydrogen transfer barrier (**TS2**) relative to *n*-propyl + O_2

	ΔE_e(ROHF)	+δ [ZAPT2]	+δ [ROCCSD]	+δ [ROCCSD(T)]	+δ [ROCCSDT]	+δ [UCCSDT(Q)]	NET
6-31G*	+31.92	–20.17	–2.21	–2.92	–0.07	–0.04	+6.50
cc-pVDZ	+31.03	–18.95	–2.14	–3.32	–0.02	[–0.04]	[+6.57]
cc-pVTZ	+30.40	–24.92	–0.41	–4.32	[–0.02]	[–0.04]	[+0.69]
cc-pVQZ	+30.72	–26.75	+0.04	–4.58	[–0.02]	[–0.04]	[–0.63]
cc-pV5Z	+30.75	[–27.40]	[+0.21]	[–4.68]	[–0.02]	[–0.04]	[–1.18]
CBS LIMIT	[+30.73]	[–28.08]	[+0.38]	[–4.77]	[–0.02]	[–0.04]	[–1.81]

FC-ROCCSD(T)/cc-pVTZ reference geometries

$\Delta E_{final} = \Delta E_e(\text{FPA}) + \Delta\text{ZPVE (harm)} + \Delta(\text{rel}) + \Delta(\text{core}) = -1.81 + 2.01 + 0.14 + 0.03 =$ **+0.37 kcal mol^{-1}**

[a] See footnote for Table 1.

5. Anharmonic Vibrational Force Field of Triacetylene

Linear polyatomic hydrocarbons, beginning with acetylene, participate in a wide array of combustion processes and have been the subject of extensive theoretical and experimental investigations. In combustion environments, diacetylene is postulated to form by the reaction of ethynyl radical (C_2H) with acetylene, ejecting a hydrogen atom. Higher molecular weight alkynes, such as triacetylene and tetraacetylene, may be created from further reactions with the ethynyl radical.

Given the general importance of polyyne compounds, we have computed the anharmonic force fields of the paradigmatic acetylene, diacetylene, and triacetylene molecules. We have worked to support the spectroscopic examination of triacetylene in a slit jet supersonic discharge carried out by the Nesbitt research group (JILA & Univ. of Colorado). To conclusively assign the ν_5 Π-Π hot band progressions built on the ν_{12} symmetric CC bend, we computed vibration-rotation interaction constants (α_i) at the CBS limit of CCSD(T). Our predicted value of α_{12} = –5.08 $\times$ 10^{-5} cm^{-1} was in fantastic agreement with experiment (–4.98 $\times$ 10^{-5} cm^{-1}) and further allowed for the confirmation of several recently assigned hot bands of triacetylene. Interestingly, the need for a definitive CCSD(T)/CBS force field requiring over 3000 energy points followed from the highly unusual prediction of *negative* diagonal quartic force constants for linear bending modes at the CCSD(T)/cc-pCVTZ level of theory. While the number of anomalous quartic force constants was reduced with use of the cc-pCVQZ basis set, it was necessary to push to the CBS limit to fully eliminate this problem. The observation of this type of basis set sensitivity on anharmonic force fields breaks new ground, and forthcoming research will examine the origin of this problem and possible issues that may arise from the use of popular F12 methods to accelerate basis set convergence.

6. Pushing the Envelope in Computing Vibronic Band Origins of Peroxy Radicals

The chemistry of peroxy radicals is pervasive in combustion. In engine cylinders, the promotion of auto-ignition reactions within the region of low-temperature "end gases" is dependent on the reactivity of RO_2 species. Of particular concern is isomerization and further reaction with O_2 as well as fragmentation to yield additional radical equivalents. Often, the $\tilde{B} \leftarrow \tilde{X}$ electronic transition is employed to monitor transient peroxy species (RO_2) formed in combustion experiments, including shock-tube detonations. This electronic excitation has a high molar absorptivity but is minimally dependent on the structure of the R group. Among others, the Miller group at Ohio State University has examined the alternative $\tilde{A} \leftarrow \tilde{X}$

transition. This excitation has a much lower absorptivity because it corresponds adiabatically to a forbidden transition between the triplet and singlet states of diatomic O_2. Nonetheless, the $\tilde{A} \leftarrow \tilde{X}$ transition has the advantage that it is a sensitive probe of the structure *and* conformation of the R group.

Future experimental work aimed at disentangling peroxy radical processes can leverage the $\tilde{A} \leftarrow \tilde{X}$ vibronic transition to determine conformer ratios and concentrations, assuming that band origins and relative intensities are known *a priori*. As a proof-of-concept, we computed the $T_0\left(\tilde{A} \leftarrow \tilde{X}\right)$ band origin for methylperoxy radical using coupled cluster theory with up to full quadruples, combined with extrapolation to the CBS limit. Additionally, the anharmonic zero-point vibrational energy was obtained from quartic force fields computed for both the ground- and excited-state potential energy surfaces. In this manner we were able to compute a purely theoretical value of $T_0\left(\tilde{A} \leftarrow \tilde{X}\right)$ = 7374 cm^{-1}. Remarkably, this theoretical prediction falls within 9 cm^{-1} of the best experimental value, 7382.8 ± 0.5 cm^{-1}. Given that conformer changes have been shown to affect $T_0\left(\tilde{A} \leftarrow \tilde{X}\right)$ of peroxy radicals by 50-100 cm^{-1}, it is clear that by pushing the envelope of current electronic structure methods, theory can provide conclusive spectroscopic band origins for combustion diagnostics.

7. Intramolecular Dispersion and Decomposition of Electron Correlation

Dispersion interactions play essential roles in many areas of chemistry, but their effects are often masked and enigmatic. An increasing appreciation of dispersion phenomena has arisen in recent years as electronic structure methods have been applied to larger and more diverse molecular systems. Persistent failures of popular density functionals and some wave function methods have highlighted the difficulties of accurately treating dispersion effects. Emerging concepts can used to explain the influence of dispersion on the thermochemistry of large hydrocarbons, including fuels most important to combustion technologies. A critical observation is that electron correlation is largely responsible for the relative stability of

branched alkanes, suggesting that this phenomenon is a manifestation of *intramolecular* dispersion effects.

Our research has developed a new approach to quantifying both inter- and intramolecular *dispersion*. We have implemented a rigorous method for decomposing and analyzing the electron correlation energy in molecular systems as a function of interelectronic distance. The method not only provides new insights into the fundamental chemical physics of electron correlation but also promises improved ways to understand and quantify dispersion energy in large hydrocarbons. There are several notable merits of our method: (1) specification of fragments within a molecule is not required; (2) it is independent of atomic orbital basis set and works best in the complete basis set limit; (3) it is based on rigorous wave function solutions to the Schrödinger equation, not density functional theory or simple analytic models; (4) it extracts fundamental properties of the exact wave function; (5) it depends fundamentally on what the electrons are doing, not where the nuclei are; (6) it does not require orbital localization, and indeed is orbital invariant; and (7) it does not require computations on artificial fragments. The key concept is to divide the Coulomb operator for electron-electron repulsion into short- and long-range components by means of new and sharper switching functions. We have used the infrastructure of our PSI4 quantum chemistry package to efficiently program the dissected two-electron integrals via recursive algorithms.

To clarify our methodology, let us consider the standard spin-orbital expression for the CCSD correlation energy ($\varepsilon_{\mathrm{CCSD}}$),

$$\varepsilon_{\mathrm{CCSD}} = \sum_{ia} f_{ia} t_i^a + \frac{1}{4} \sum_{ijab} \langle ij || ab \rangle \left(t_{ij}^{ab} + t_i^a t_j^b - t_i^b t_j^a \right) \tag{7.1}$$

where the Fock matrix elements are

$$f_{ia} = h_{ia} + \sum_{k}^{\mathrm{occ}} \langle ik || ak \rangle \ , \tag{7.2}$$

h_{ia} and $\langle ij || mn \rangle$ are the usual one-electron and antisymmetrized two-electron integrals, respectively, (t_i^a, t_{ij}^{ab}) represent the cluster amplitudes for connected (single, double)

excitations, and the indices denote occupied (*i*, *j*, *k*) and virtual (*a*, *b*) molecular spin orbitals. To provide a clean separation of long- and short-range electron correlation, the conventional coupled-cluster wave function is first converged to fix the cluster amplitudes. Our approach then back-transforms the cluster amplitudes into the atomic-orbital basis, indexed by μ, ν, λ, and σ:

$$t_{\mu\nu} = \sum_{ia} t_i^a C_{\mu i} C_{\nu a} \tag{7.3}$$

$$t_{\mu\nu\lambda\sigma} = \sum_{ijab} t_{ij}^{ab} C_{\mu i} C_{\nu a} C_{\lambda j} C_{\sigma b} \tag{7.4}$$

where the $C_{\mu m}$ quantities are the molecular orbital coefficients. Accordingly, the correlation energy can be written in the form

$$\varepsilon_{\mathrm{CCSD}} = \sum_{\mu\nu} t_{\mu\nu} h_{\mu\nu} + \frac{1}{2} \sum_{\mu\nu\lambda\sigma} \left(\mu\nu\middle|\lambda\sigma\right)\left[t_{\mu\nu\lambda\sigma} + t_{\mu\nu}\left(t_{\lambda\sigma} + 2P_{\lambda\sigma}\right) - t_{\mu\lambda}\left(t_{\nu\sigma} + 2P_{\nu\sigma}\right)\right] \tag{7.5}$$

where $P_{\lambda\sigma}$ is the Hartree-Fock one-electron density matrix. This expression explicitly involves the one- and two-electron integrals $[h_{\mu\nu}, (\mu\nu\,|\,\lambda\sigma)]$ in the AO basis, with the expense of a single N^5 step to back-transform the cluster amplitudes.

In the next stage we divide the $(\mu\nu\,|\,\lambda\sigma)$ integrals into short- and long-range parts based on some variable interelectronic cutoff distance r_x,

$$\left(\mu\nu\middle|\lambda\sigma\right) = \left(\mu\nu\middle|\lambda\sigma\right)_{r_{12}<r_x} + \left(\mu\nu\middle|\lambda\sigma\right)_{r_{12}>r_x} \tag{7.6}$$

which provides a well-defined separation of the correlation energy as

$$\varepsilon_{\mathrm{CCSD}}^{\mathrm{short}} = \sum_{\mu\nu} t_{\mu\nu} h_{\mu\nu} + \frac{1}{2} \sum_{\mu\nu\lambda\sigma} \left(\mu\nu\middle|\lambda\sigma\right)_{r_{12}<r_x}\left[t_{\mu\nu\lambda\sigma} + t_{\mu\nu}\left(t_{\lambda\sigma} + 2P_{\lambda\sigma}\right) - t_{\mu\lambda}\left(t_{\nu\sigma} + 2P_{\nu\sigma}\right)\right] \tag{7.7}$$

and

$$\varepsilon_{\mathrm{CCSD}}^{\mathrm{long}} = \frac{1}{2} \sum_{\mu\nu\lambda\sigma} \left(\mu\nu\middle|\lambda\sigma\right)_{r_{12}>r_x}\left[t_{\mu\nu\lambda\sigma} + t_{\mu\nu}\left(t_{\lambda\sigma} + 2P_{\lambda\sigma}\right) - t_{\mu\lambda}\left(t_{\nu\sigma} + 2P_{\nu\sigma}\right)\right] . \tag{7.8}$$

Our initial scheme achieved a splitting of the electron-electron repulsion integrals by means of general classes of relatively sharp switching functions represented as transforms of the error function $\mathrm{erf}(\omega r_{12})$. Evaluation of the $(\mu\nu\,|\,\lambda\sigma)_{r_{12}<r_x}$ and $(\mu\nu\,|\,\lambda\sigma)_{r_{12}>r_x}$ integrals required the

computation of sets of $\left(\mu\nu\left|r_{12}^{-1}\,\mathrm{erf}(\omega r_{12})\right|\lambda\sigma\right)$ integrals for 10–20 different values of the parameter ω. These integral evaluations only scale as N^4 and are inexpensive compared to the N^6 requirements already invested to obtain the CCSD wave function. In our most recent work, we were able to derive and program analytic expressions for the two-electron integrals involving the Heaviside step function as the switching function. The analytic formulas proved that the integrations over the Heaviside function have no problems with discontinuities or cusps because the underlying electron density profiles are smooth. With this advancement we can now employ a switching function of the maximum possible sharpness.

To demonstrate the wealth of information that can be gained by our dispersion analyses, some firstfruits of the method are shown for the benzene dimer in Figure 5. The computations were performed at the aug-cc-pVDZ CCSD level of theory near the optimum geometry of the complex (3.7 Å ring separation). The plot reveals how the correlation energy contribution to the binding energy changes with the cutoff distance r_x for electron-electron interactions. The asymptote of the plot ($r_x \rightarrow \infty$) shows that about 6 kcal mol^{-1} of dispersion stabilization is achieved when all electron correlation is included. Of course, the repulsive Hartree-Fock component of the interaction energy cancels about half of this stabilization. A striking aspect of the plot is that the dispersion stabilization is much stronger (11 kcal mol^{-1}) if the electrons are allowed to interact only up to a distance of 6 bohr. The minimum in the curve means that electron correlation over distances less than 6 bohr always increases the binding energy. Conversely, electron correlation over distances between than 6 and 11 bohr *decreases* the binding energy! In other words, the longer range correlations are actually repulsive, contrary to current understandings. Our analysis confirms that the benzene dimer is held together by dispersion; however, the attraction comes exclusively from short and intermediate range electron correlation, presumably between the π electrons of each ring.

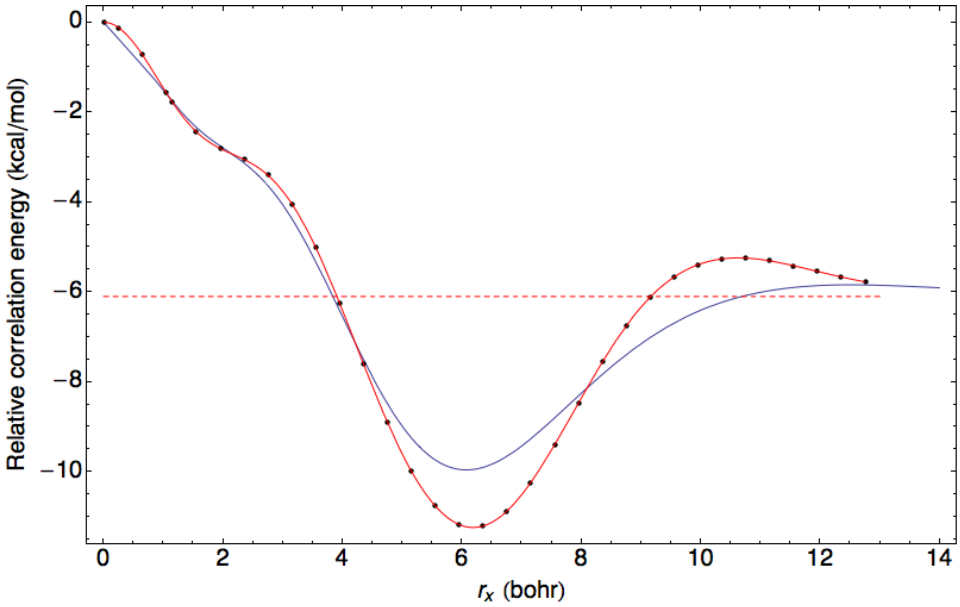

Figure 5. Electron-electron distance (r_x) dependence of the aug-cc-pVDZ CCSD correlation energy contribution to the binding energy (in kcal mol^{-1}) of the benzene dimer at a ring-separation of 3.7 Å. The red curve results from splitting the Coulomb operator with the Heaviside step function to provide the maximum possible resolution. The blue curve shows previous results we obtained by employing a hyperbolic tangent attenuator of less resolution represented as an expansion in error functions.

In all of the applications we have executed thus far, the dependence of the relative electron correlation energy ($\Delta\varepsilon$) on the cutoff distance (r_x) for electron-electron interactions has the same general structure as exhibited for benzene dimer. The corresponding $\Delta\varepsilon(r_x)$ curve for the prototypical argon dimer is shown in Figure 6, as generated with the Heaviside step function. The dispersion stabilization of the dimer is strongest near r_x = 5.5 bohr. The region of destabilizing interactions runs from 5.5 to about 9.0 bohr. Finally, the longest range interactions provide about 0.2 kcal mol^{-1} of stabilization. The consistency of the shape of $\Delta\varepsilon(r_x)$ curves observed in our studies suggests that certain salient features may provide valuable diagnostics of dispersion: the depth, position, and curvature of the intermediate range minimum; the height, position, and curvature of the long range maximum; and the points of intersection with the asymptotic binding energy.

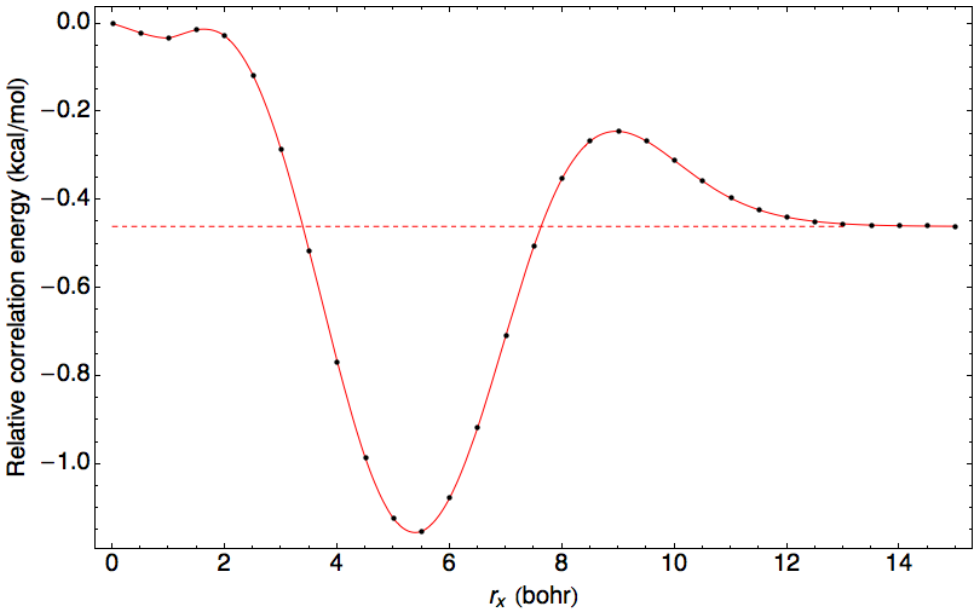

Figure 6. Electron-electron distance (r_x) dependence of the aug-cc-pVQZ CCSD(T) correlation energy contribution to the binding energy (kcal mol^{-1}) of argon dimer at 3.76 Å separation.

Another revealing signature of dispersion is shown in Figure 7 for the argon dimer. The abscissa in this plot is the same cutoff distance used before; however, the ordinate is the total correlation energy rather than the contribution of this quantity to the binding energy. Superimposed on the $\varepsilon(r_x)$ curve for Ar_2 is the corresponding curve for two isolated Ar atoms. The difference between the two curves would yield the function plotted above in Figure 6, which clearly demonstrated that dispersion cannot be understood *simplistically* as long-range electron correlation. A striking feature in Figure 7 is that the $\varepsilon(r_x)$ curves for Ar_2 and 2 Ar are virtually identical for r_x less than 4.5 bohr. The manner in which the two curves depart for larger distances does provide a fingerprint of the dispersion in this system and reveals how dispersion can be properly understood as long-range electron correlation. This research suggests that $\varepsilon(r_x)$ curves should be generated for all atoms to provide reference systems for molecular analyses. In brief, by taking an $\varepsilon(r_x)$ curve for a molecule and comparing with the sum of the corresponding curves for the constituent atoms, a revealing analysis of the

molecular electron correlation results. For distances larger than the atomic realm, the molecular $\varepsilon(r_x)$ curve relative to its atomic reference components should help solve the thorny question of how to define intramolecular dispersion.

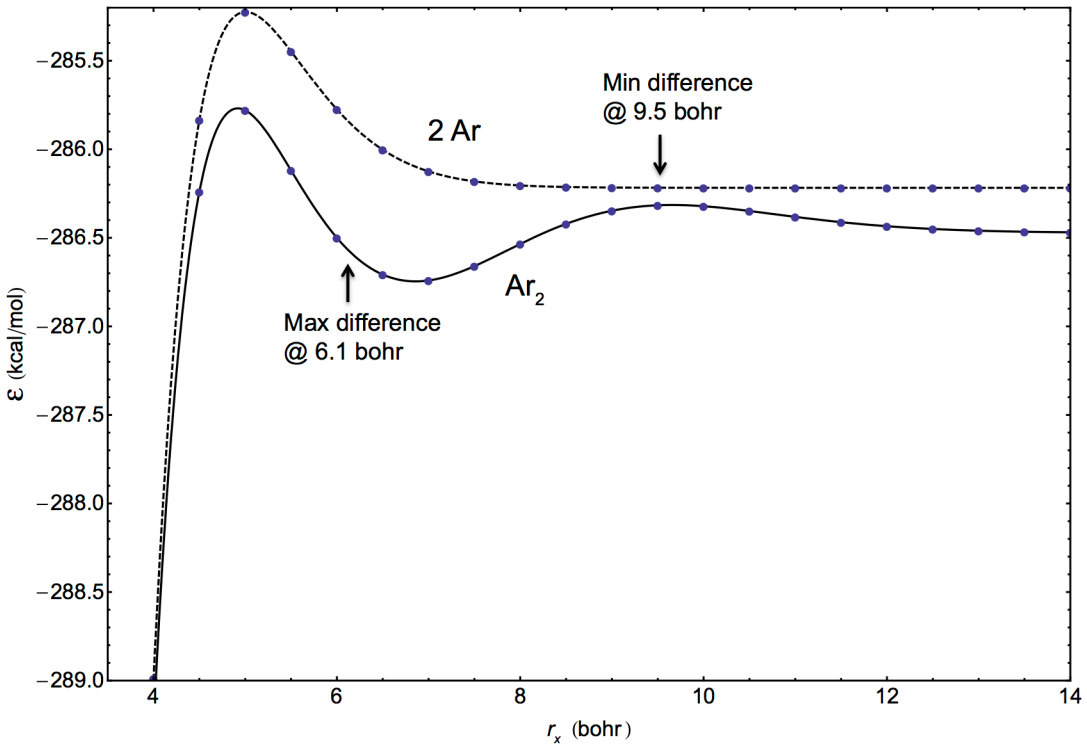

Figure 7. Electron-electron distance (r_x) dependence of the aug-cc-pVTZ CCSD(T) correlation energy of argon dimer at 3.76 Å separation as compared to that of two isolated argon atoms.

CONCLUSIONS

(1) Significant advances have been achieved in integral approximations and screening for studies on large molecules. A new density fitting scheme that leads to smooth and artifact-free potential energy surfaces was successful in benchmarking studies on 200 large molecules, including up to 140 atoms. A new estimator for three-center two-particle Coulomb integrals yields increased efficiency in reduced-scaling one- and many-body electronic structure theories.

(2) Within the framework of the Bogoliubov quasiparticle Hamiltonian, we have derived and begun to implement a multireference variant of $CEPA_0$ (MR-$CEPA_0$). Our Bogoliubov MR-$CEPA_0$ (BMR-$CEPA_0$) requires only the one-particle density matrix of the reference wave function and will provide a simple, effective extension of $CEPA_0$ in the presence of strong correlation.

(3) As an alternative approach for incorporating explicit correlation into electronic wave functions, we have implemented a canonical transcorrelated (CT) Hamiltonian method that has the benefit of having no more computational complexity (only one- and two-body interactions) than conventional approaches. We have examined the dependence of the CT correlation energy with respect to Slater geminal exponents and compared CT results to those of popular F12 methods for small systems. Continuing work will focus on using the CT Hamiltonian with higher-order coupled cluster methods.

(4) Definitive theoretical methods have been employed in a comprehensive examination of the multichannel *n*-propyl + O_2 reaction, an important model of larger combustion systems. Focal point analyses (FPA) extrapolating to the *ab initio* limit were performed based on explicit quantum chemical computations with electron correlation treatments through CCSDT(Q) and basis sets up to cc-pV5Z. All reaction species and transition states were fully optimized at the rigorous CCSD(T)/cc-pVTZ level of theory, providing substantial improvements over existing DFT geometric structures. A mixed Hessian methodology was devised and benchmarked that essentially makes the computations of CCSD(T)/cc-pVTZ vibrational frequencies feasible and thus provides critical improvements to zero-point vibrational energies.

(5) Groundbreaking CCSD(T)/CBS anharmonic force fields have been computed for the diacetylene and triacetylene molecules. Our anharmonic predictions have supported the spectroscopic examination of triacetylene in a slit jet supersonic discharge, allowing conclusive assignments of new vibrational progressions. The triacetylene vibrational anharmonicity problem showed extreme basis set sensitivity in that *negative* diagonal quartic force constants are predicted for linear bending modes even at the CCSD(T)/cc-pCVQZ level of theory. Popular F12 methods to accelerate basis set convergence are not realiable in this application, and pushing the computation to the CBS limit proves essential.

(6) Future experimental research aimed at disentangling peroxy radical chemistry can leverage $\tilde{A} \leftarrow \tilde{X}$ vibronic transitions to determine conformer ratios and concentrations. We have proved that state-of-the-art electronic structure theory can predict highly accurate $\tilde{A} \leftarrow \tilde{X}$ band origins by studying methylperoxy radical using coupled cluster theory through CCSDTQ with extrapolations to the CBS limit. Remarkably, our theory reproduced the best experimental value, T_0 = 7382.8 ± 0.5 cm^{-1}, to within 9 cm^{-1}.

(7) A new method has been developed to quantify both inter- and intramolecular dispersion by decomposing and analyzing the electron correlation energy in molecular systems as a function of interelectronic distance. The method not only provides new insights into the fundamental chemical physics of electron correlation but also promises improved ways to understand and quantify dispersion energy in large hydrocarbons. The new method has several notable merits: (a) conceptualization of fragments within a molecule is not required; (b) there are no restrictions on the atomic orbital basis set, and complete basis set limits are well defined; (c) rigorous wave function solutions to the Schrödinger equation provide the foundation, not density functional theory or simple analytic models; (d) the analysis depends on fundamental properties that can be extracted from the exact wave function; (e) the fundamental focus is on what the electrons are doing, not where the nuclei are; (f) no orbital localization is required, and orbital invariance is maintained; and (g) artificial fragments do not have to be computed.

REFERENCES

1. A. Gao, G. Li, B. Peng, Y. Xie, and H. F. Schaefer, "The Symmetric Exchange Reaction OH + $H_2O \rightarrow H_2O$ + OH: Convergent Quantum Mechanical Predictions," *J. Phys. Chem. A* **120**, 10223 (2016).
2. A. W. Ray, J. Agarwal, B. B. Shen, H. F. Schaefer, and R. E. Continetti, "Energetics and Transition State Dynamics of the F + $HOCH_3 \rightarrow$ HF + OCH_3 Reaction," *Phys. Chem. Chem. Phys.* **18**, 30612 (2016).
3. X. Wang, J. Agarwal, and H. F. Schaefer, "Characterizing a Nonclassical Carbene with Coupled Cluster Methods: Cyclobutylidene," *Phys. Chem. Chem. Phys*. **18**, 24560 (2016).
4. P. F. Franke, D. P. Tabor, C. P. Moradi, G. E. Douberly, J. Agarwal, H. F. Schaefer, and E. L. Sibert, "Infrared Laser Spectroscopy of the *n*-Propyl and *i*-Propyl Radicals: Stretch-Bend Fermi Coupling in the Alkyl CH Stretch Region," *J. Chem. Phys*. **145**, 224304 (2016).
5. M. Estep and H. F. Schaefer, "The Methylsulfinyl Radical CH_3SO Examined," *Phys. Chem. Chem. Phys.* **18**, 22293 (2016).
6. P. R. Hoobler, J. M. Turney, and H. F. Schaefer, "Investigating the Ground-State Rotamers of the *n*-Propylperoxy Radical," *J. Chem. Phys*. **145**, 17430 (2016).
7. W. D. Allen, H. Quanz, and P. R. Schreiner, "Polytriangulane," *J. Chem. Theory Comput.* **12**, 4707-4716 (2016).
8. K. V. Murphy, W. J. Morgan, Z. Sun, H. F. Schaefer, and J. Agarwal, "Thioformaldehyde S-Sulfide, Sulfur Analogue of the Criegee Intermediate: Structures, Energetics, and Rovibrational Analysis," *J. Phys. Chem. A* **121**, 998 (2017).
9. E. Castro, G. Avila, S. Manzhos, J. Agarwal, H. F. Schaefer, and T. Carrington, "Applying a Smolyak Collocation to Cl_2CO," *Mol. Phys*. **115**, 1775 (2017).
10. D. S. Hollman, H. F. Schaefer, and E. F. Valeev, "Fast Construction of the Exchange Operator in an Atom-Centered Basis with Concentric Atomic Density Fitting," *Mol. Phys.* **115**, 2065 (2017).
11. H. I. Rivera-Arrieta, J. M. Turney, and H. F. Schaefer, "Structural Distortions Accompanying Non-Covalent Interactions: Methane-Water, the Simplest C-H Hydrogen Bond," *J. Chem. Theory Comput*. **13**, 1478 (2017).

12. K. V. Murphy, H. F. Schaefer, and J. Agarwal, “Phosgene at the Complete Basis Set Limit of CCSDT(Q): Molecular Structure and Rovibrational Analysis,” *Chem. Phys. Lett.* **683**, 12 (2017).
13. K. B. Moore, J. M. Turney, and H. F. Schaefer, “The Fate of the *Tert*-Butyl Radical in Low-Temperature Autoignition Reactions,” *J. Chem. Phys.* **146**, 194304 (2017).
14. R. M. Parrish, L. A. Burns, D. G. A. Smith, A. C. Simmonett, A. E. DePrince, E. G. Hohenstein, U. Bozkaya, A. Y. Sokolov, R. D. Remigio, R. M. Richard, J. F. Gonthier, A. M. James, H. R. McAlexander, A. Kumar, M. Saitow, X. Wang, B. P. Pritchard, P. Verma, H. F. Schaefer, K. Patkowski, R. A. King, E. F. Valeev, F. A. Evangelista, J. M. Turney, T. D. Crawford, and C. D. Sherrill, “PSI4 1.1: An Open-Source Electronic Structure Program Emphasizing Automation, Advanced Libraries, and Interoperability,” *J. Chem. Theory Comput.* **13**, 3185 (2017).
15. A. M. Launder, J. M. Turney, J. Agarwal, H. F. Schaefer, “Ethylperoxy Radical: Approaching Spectroscopic Accuracy via Coupled-Cluster Theory,” *Phys. Chem. Chem. Phys.* **19**, 15715 (2017).
16. S. K. Pandey, D. Manogaran, S. Manogaran, and H. F. Schaefer, “Quantification of Hydrogen Bond Strength Based on Interaction Coordinates: A New Approach,” *J. Phys. Chem. A* **121**, 6090 (2017).
17. M. L. Estep, W. J. Morgan, A. T. Winkles, A. S. Abbott, N. A. Villegas-Escobar, J. W. Mullinax, W. E. Turner, X. Wang, J. M. Turney, and H. F. Schaefer, “Radicals Derived from Acetaldehyde and Vinyl Alcohol,” *Phys. Chem. Chem. Phys.* **19,** 27275 (2017).
18. K. B. Moore, K. Sadeghian, C. D. Sherrill, C. Ochsenfeld, and H. F. Schaefer, “C—H ⋯ O Hydrogen Bonding. The Prototypical Methane-Formaldehyde System: A Critical Assessment,” *J. Chem. Theory Comput.* **13**, 5379 (2017).
19. M. A. Bartlett, T. Liang, L. Pu, H. F. Schaefer, and W. D. Allen, “The Multichannel *n*-Propyl + O_2 Reaction Surface: Definitive Theory on a Model Hydrocarbon Oxidation Mechanism,” *J. Chem. Phys*. **148**, 094303: 1–18 (2018).

Final Technical Report DOE-UGA-15512

University of Georgia Research Foundation